NMR visualization of displacement correlations for flow in porous media

A. A. Khrapitchev,[1] S. Stapf,[2] and P. T. Callaghan[1,*]
[1]*School of Chemical and Physical Sciences, Victoria University, P.O. Box 600, Wellington, New Zealand*
[2]*Lehrstuhl für Makromolekulare Chemie, ITMC, RWTH Aachen, Worringerweg 1, D-52074 Aachen, Germany*
(Received 1 February 2002; revised manuscript received 12 July 2002; published 20 November 2002)

The temporal correlations of velocities for both water and a water-glycerol mixture flowing through a random packings of monodisperse spherical particles have been investigated using two-dimensional nuclear magnetic resonance methods. By combining various flow rates, fluid viscosities, and bead sizes, a wide range of flow parameters has been covered, the dimensionless Peclet number ranging from 100 to 100 000. The velocity exchange spectroscopy (VEXSY) technique has been employed to measure the correlation between velocities during two intervals separated from each other by a mixing time τ_m. This time is made both large and small compared with the time constant τ_c, required for a fluid element possessing the average flow velocity to cover a distance equal to the characteristic size in the system, the bead diameter. The two-dimensional conditional probability of displacement resulting from the VEXSY method reveals the existence of different ''subensembles'' of molecules, including a slow moving pool whose displacement is dominated by Brownian motion, an intermediate ensemble whose velocities change little over the mixing time, and a fast flowing ensemble which loses correlation due to mechanical dispersion. We find that that the approach to asymptotic dispersion, as τ_c/τ_m increases, depends strongly on the Peclet number, the deviation of the velocity autocorrelation function from a monoexponential Ornstein-Uhlenbeck process becoming more pronounced with increasing Peclet number.

DOI: 10.1103/PhysRevE.66.051203 PACS number(s): 47.15.−x, 81.05.Rm, 82.56.Fk, 47.80.+v

INTRODUCTION

The physics of fluid dispersion in porous media provides an interesting example of processes involving both coherent and stochastic dynamics in which a crossover between behaviors is marked by characteristic time and length scales. These physical phenomena are important in understanding a range of natural and industrial processes, such as perfusion in biological tissue, transport in geological media [1–3], two-phase flow in oil recovery [4,5], molecular separation using chromatographic methods [6–8], and the behavior of packed bed reactors [9,10]. Nuclear magnetic resonance (NMR) has the considerable advantage of being a noninvasive method providing chemical selectivity and a large spectrum of contrasting parameters. For many years, NMR pulsed-field gradient (PFG) techniques have been a powerful tool for the investigation of transport processes. Recently, it has been shown that NMR methods are particularly effective in studying dispersion, especially because the technique allows a well-defined displacement propagator to be measured [11,12]. Furthermore, because NMR relies on a time sequence of radio-frequency and magnetic field gradient encoding pulses, it is possible to design sequences that permit the study of the time dependence of displacements. Given a judicious choice of pore dimensions and flow rates, these time dependencies can encompass the characteristic time for the fluid to move across one pore. When combined with spatial localization techniques, NMR imaging allows flow visualization [13–18]. However, imaging methods generally require a trade-off against other important parameters of interest, such as the signal-to-noise ratio, and the minimum period of time over which flow displacements may be observed. Furthermore, where overall ensemble properties of the flow field are sought, the need for spatial localization is obviated. Thus, the use of NMR imaging is not always necessary or optimal, given the specific fluid parameters being sought.

A number of NMR methods focus particularly on temporal characteristics of the velocity field. These include double-pulsed gradient spin echo NMR in which the velocity autocorrelation function is measured directly over times ranging from milliseconds to seconds [19,20], frequency domain modulated gradient NMR in which the Fourier transform of the velocity autocorrelation function is measured in the frequency range of 10 Hz to 10 kHz [21,22], and velocity exchange spectroscopy (VEXSY [23] and its closely related technique, SERPENT [24,25]) in which temporal correlations in the velocity field are obtained as a two-dimensional map, the time variable being the so-called ''exchange time'' over which velocity variations are compared, and whose values, like that of double pulsed gradient spin echo NMR, range from a few milliseconds to seconds. It has been shown that in the VEXSY experiment, special NMR pulse sequences are necessary if the method is to work well over a wide range of exchange times [26]. In this paper we apply velocity exchange spectroscopy to a study of dispersive flow in a model porous medium of randomly packed spheres, and under a wide range of Peclet numbers, bead diameters, and exchange times. We compare the results of our experiments with theoretical predictions of flow through a similar system with corresponding fluid motion parameters obtained by computer simulations.

This paper serves three purposes. First we seek to demonstrate the potential for the NMR VEXSY experiment to

*Corresponding author. FAX: +64-4-4635237. Email address: paul.callaghan@vuw.ac.nz

reveal the temporal character of the complex velocity distribution associated with fluid dispersion. In doing so we shall indicate the limitations of the method as well as its particular strengths. Second, we will show how VEXSY can be used to obtain the two-dimensional conditional probability for displacements over two separated time intervals. Finally, we will use the method to examine flow behavior in a well-defined system and to investigate the rate of approach to asymptotic behavior.

The conditional probability plots that we show here exhibit complex structure. While we are unable to provide a detailed quantitative explanation, we find similar structure in numerical simulations performed on a similar theoretical structure under similar conditions. We are able to draw qualitative conclusions from our study. In particular, we shall show that there exists more than one characteristic time for the transition to asymptotic conditions and that these times are closely related to details of the steady state velocity spectrum.

DISPERSION IN POROUS MEDIA

In the theory of dispersion, it is customary to define the fluctuation in the Lagrangian velocity field, $\mathbf{u}(t)=\mathbf{v}(t)-\mathbf{V}$, where $\mathbf{v}$ is the local instantaneous velocity and $\mathbf{V}$ is an averaged velocity defined by $\mathbf{V}=\lim_{t\to\infty}\langle\mathbf{v}\rangle$, where the ensemble average $\langle\ \rangle$, is taken over the distribution of velocity fields [27,28] localized in space. Notice that the long-time limit is taken with respect to the correlation time of the velocity fluctuations [29]. The asymptotic dispersion tensor is then described by [19]

$$D^*=\lim_{t\to\infty}\mathcal{S}\int_0^t\langle\mathbf{u}(\tau)\mathbf{u}(0)\rangle d\tau, \tag{1}$$

where $\mathcal{S}(\mathbf{A})=\frac{1}{2}(\mathbf{A}+\mathbf{A}^T)$. $\langle\mathbf{u}(t)\mathbf{u}(0)\rangle$ is the velocity autocorrelation function.

We will be concerned in this paper with flow in a porous medium contained within a cylindrical tube of constant cross section. We denote the component of $\mathbf{v}$ along the direction of mean flow as v and note that for a porous medium $\langle v\rangle=\langle v_{\mathrm{tube}}\rangle/\phi$, where $\langle v_{\mathrm{tube}}\rangle$ is the mean velocity deduced from the volume flow rate in the absence of the porous medium and ϕ is the porosity of the structure.

Equation (1) describes the ''asymptotic'' or long time scale ''steady state'' dispersion. The meaning of the long time limit is that t must exceed the correlation time of the velocity fluctuations. Note that the trace of this tensor describes a scalar dispersion coefficient which is simply related to the mean-squared displacements via

$$\mathrm{Tr}(\mathbf{D}^*)=\lim_{t\to\infty}\frac{1}{2}\frac{d\sigma^2(t)}{dt}, \tag{2}$$

where $\sigma^2(t)=\langle[\mathbf{r}(t)-\langle\mathbf{r}(t)\rangle]^2\rangle$ is the positional variance. Equation (2) provides an alternative definition of the asymptotic dispersion.

At measurement times in the preasymptotic regime, the dispersive behavior is considerably more complex. Here anomalous dispersion due to heterogeneity of the porous medium requires a nonlocal formulation in which the nonlocal dispersion tensor is dependent on time interval and displacement [27,28], and given by

$$D^*(\mathbf{r}-\mathbf{r}',t-t')=\langle\mathbf{u}(\mathbf{r},t)P(\mathbf{r},t|\mathbf{r}',t')\mathbf{u}(\mathbf{r}',t')\rangle, \tag{3}$$

where $P(\mathbf{r},t|\mathbf{r}',t')$ is a transition probability of a tracer from $\mathbf{r}$ at t to $\mathbf{r}'$ at t' and is governed by the microscale advection-diffusion equation at each point in the medium. The local dispersion tensor is obtained from the nonlocal form by integrating over $\mathbf{r}'$ and t' in Eq. (3). Its trace reproduces the local dispersion coefficient.

In our NMR measurements, we will generally be concerned with diagonal elements of the dispersion tensor in which relevant components of velocity are determined by the applied magnetic field gradient direction in a pulsed gradient spin echo NMR experiment.

A crucial parameter in defining the temporal structure of the velocity field is the correlation time τ_c corresponding to the duration of flow around a characteristic length scale. For a medium with pore size or pore spacing given by size d, the correlation time may be written as

$$\tau_c=\frac{d}{\langle v\rangle}. \tag{4}$$

In this work we shall describe flow in a packed bed of monodisperse spherical beads, for which we shall take d to be given by the bead diameter. Note that the time τ_c is not the only characteristic time for porous media flow. A longer time is defined by the time to flow over the larger length scale associated with the so-called representative elementary volume (REV) [30–32]. The REV is the smallest volume containing all morphological features which exist in the porous medium with their global statistical weighting; its size is on the order of the longest correlation length, which, in our case, is determined by the packing inhomogeneity. Furthermore, given the wide distribution of velocities present in porous media flow, the notion of a unique correlation time, whatever the length scale and mean flow rate, is misleading, and we shall later generalize it by formally introducing a distribution of correlation times, $P(\tau_c)$

Another time that is important to an understanding of the process of dispersion is that required to migrate the characteristic distance by Brownian motion alone. The definition of two characteristic times leads one to a dimensionless number that characterizes the flow dynamics, the Peclet number Pe. In a porous medium Pe expresses the ratio of the time taken to diffuse across a pore to the time taken to flow across a pore, and is given by

$$\mathrm{Pe}=\frac{l\langle v\rangle}{D_0}, \tag{5}$$

where D_0 is the molecular self-diffusion coefficient. In the case of bead packs it is usual practice [33,34] to take the characteristic dimension l as being given by the effective pore diameter, defined by $l=\phi d_p/(1-\phi)$. We will assume this definition of the Peclet number throughout this paper.

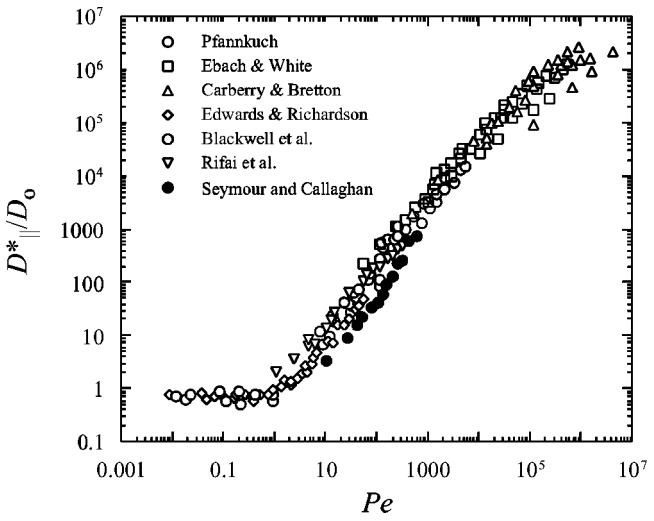

FIG. 1. Literature data for nondimensionalized longitudinal asymptotic dispersion coefficients versus Peclet number.

The mechanisms that cause dispersion are often discussed in terms of three principal processes. Mechanical dispersion is due to stochastic variations in velocity induced by advection along tortuous paths and flow bifurcations and scales as the Peclet number Pe. Diffusive (Taylor) dispersion arises from molecular diffusion across streamlines and scales as Pe^2. Holdup dispersion arises from the presence of dead end pores, and scales as Pe lnPe [32–35].

In the asymptotic regime, where the observation time greatly exceeds the longest correlation time, D^* is homogeneous (spatially independent of length scales exceeding the REV) and stationary (observation time independent). The dimensionless asymptotic dispersion D^*/D_0 has been observed to follow a universal curve as shown in Fig. 1. For $\mathrm{Pe}\ll 1$, the microscopic Brownian motion dominates D^*. For $\mathrm{Pe}\gg 1$ an approximate power law behavior, $D^*/D_0 \sim \mathrm{Pe}^{\alpha}$, is observed with $\alpha \sim 1.2$ for flow in packings of spherical particles (this is also the result of numerical simulations [36]), gradually reducing with increasing Pe, indicating superposed dispersive mechanisms with mechanical dispersion dominating at the highest Pe.

In attempting to describe the spatially averaged preasymptotic dispersion, we shall adopt a phenomenological approach by assuming a simple expression for the correlation function $\langle u(t)u(0)\rangle$ such as the Ornstein-Uhlenbeck process [37], which takes the exponential, stationary Gaussian Markoff form

$$\langle u(t)u(0)\rangle = \langle u^2\rangle \exp(-t/\tau_c). \tag{6}$$

Defining the NMR-measured dispersion coefficient at finite observation time t in terms of an appropriate time integral of the diffusion spectrum, this particular correlation function yields

$$D^*(t) = \langle u^2\rangle \tau_c \{1 + (\tau_c/t)[\exp(-t/\tau_c) - 1]\}, \tag{7}$$

where $\langle u^2\rangle \tau_c$ is the asymptotic value D^*. This simple expression neglects possibilities of dispersion associated with a distribution of correlation times, and in particular the longer time associated with the larger length scale of the representative elementary volume.

VELOCITY EXCHANGE SPECTROSCOPY

The elucidation by means of VEXSY, of correlations between particle velocities at two different times separated by a mixing time τ_m, is based on a double encoding of displacements. These encoding steps, in turn, are each brought about by the application of a pair of magnetic field gradient pulses of identical magnitude but alternating sign. These pulses (denoted PFG) are separated by a time Δ which we shall refer to as the velocity encoding time.

The magnetic field experienced by the nuclear spins in the sample can be decomposed into a homogeneous contribution $\mathbf{B}_0 = (0,0,B_0)$ and a spatially constant field gradient $\mathbf{g} = (\partial B_z/\partial x, \partial B_z/\partial y, \partial B_z/\partial z)$.

Consequentially, the Larmor precession frequency of a spin species of gyromagnetic ratio γ is given by

$$\omega(\mathbf{r}) = -\gamma(|\mathbf{B}_0| + \mathbf{g}\cdot\mathbf{r}) \tag{8}$$

and thus depends linearly on the position of the spins along the direction of the applied gradient **g**. If the gradient is applied in the shape of a short, rectangular pulse of duration δ, the difference in $\omega(\mathbf{r})$ becomes effective only during δ and leads to the accumulation of a phase shift

$$\phi_i = \delta\omega(\mathbf{r}_i) = -\gamma(|\mathbf{B}_0| + \mathbf{g}\cdot\mathbf{r}_i) \tag{9}$$

for the spin i being located at $\mathbf{r}_i$. If a second pulsed-field gradient of opposite effective amplitude is applied a time interval Δ later (see the pulse sequence in Fig. 2(a) [38]), a second phase shift is added with a negative weighting, and the total shift for spin i will be

$$\phi_i = \gamma\delta\mathbf{g}\cdot[\mathbf{r}_i(\Delta) - \mathbf{r}_i(0)] = \gamma\delta\mathbf{g}\cdot[\mathbf{R}_i(\Delta)], \tag{10}$$

where $\mathbf{R}_i(\Delta) = \mathbf{r}_i(\Delta) - \mathbf{r}_i(0)$ indicates the displacement for particle i during the encoding time Δ. The reduced total signal amplitude for the ensemble of spins in the sample [normalized to the signal intensity in the absence of gradients $S(0)$] is obtained by summation over all spins, equivalent to the following integral:

$$E(\mathbf{q}) = S(\mathbf{q})/S(0) = \int \overline{P}_1(\mathbf{R},\Delta)\exp[i2\pi\mathbf{q}\cdot\mathbf{R}(\Delta)]d\mathbf{R}, \tag{11}$$

where the wave vector **q** is defined as $\mathbf{q} = (2\pi)^{-1}\gamma\delta\mathbf{g}$. It is the equivalent to the wave number in scattering experiments and has the dimension of reciprocal length.

The average propagator $\overline{P}_1(\mathbf{R},\Delta)$ is given by

$$\overline{P}_1(\mathbf{R},\Delta) = \int \rho(\mathbf{r}_0)P(\mathbf{r}_0|\mathbf{r}_1,\Delta)d\mathbf{r}, \tag{12}$$

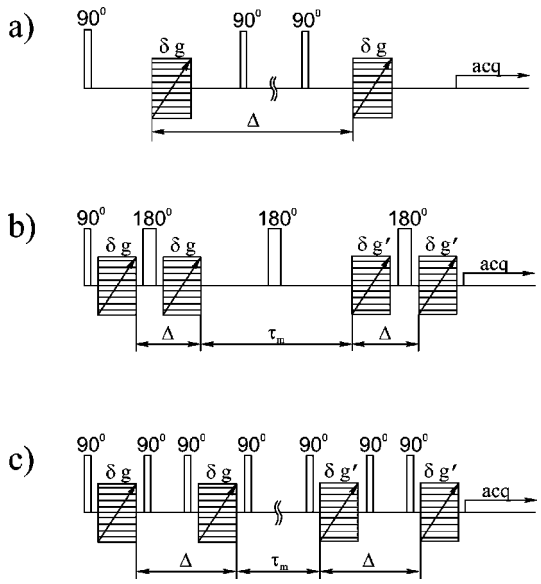

FIG. 2. (a) Schematic rf and gradient pulses sequence for a simple PGSTE NMR experiment in which the gradient pulse area δg is stepped and z storage is used for the encoding period. (b) Schematic rf and gradient pulses sequence for a general double PGSE NMR experiment in which the gradient pulse areas δg and $\delta g'$ are stepped simultaneously in 1D experiments or independently in the 2D version. (c) The same as for (b), but z storage is used for both the encoding and mixing periods.

where $\rho(\mathbf{r}_0)$ is the probability density for starting positions, while $P(\mathbf{r}_0|\mathbf{r}_1,\Delta)$ is the conditional probability for displacements from $\mathbf{r}_0$ to $\mathbf{r}_1$ in time Δ [11,12]. The average propagator $\overline{P}_1(\mathbf{R},\Delta)$ is obtained directly from Fourier transformation of the signal function $E(\mathbf{q})$ with respect to $\mathbf{q}$. It should be noted that Eq. (11) and all following Fourier relations are strictly applicable only if the duration of the gradient pulse is much smaller than the encoding time ($\delta \ll \Delta$) and if velocity fluctuations during δ remain negligible.

We note further that because the experiment is characterized by a simultaneous variation of two opposing gradient pulses, information about the initial and final position becomes lost and only the distribution of displacements is retained. Hence, neither $\rho(\mathbf{r}_0)$ nor the conditional probability for positions, $P(\mathbf{r}_0|\mathbf{r}_1,\Delta)$, is accessible. However, the experiment can, in principle, be performed in a two-dimensional way with gradients being varied independently of each other, avoiding these restrictions at the cost of increased experimental time [39].

The methods of measuring displacements by a PFG pair can be extended towards a multiple encoding of displacements by repeated application of PFG pairs, each of them adding a further phase shift to the individual spin, which is proportional to its motion during the different encoding intervals [40–42]. In particular, a twofold encoding, following the scheme shown in Figs. 2(b) and 2(c), measures displacements of particles being accumulated during the first *and* the second encoding interval, both of which have been chosen as having the same duration Δ for symmetry reasons. The total signal amplitude can now be written as

$$E(\mathbf{q}) = \int\int \overline{P}_2(\mathbf{R}_1,\Delta;\mathbf{R}_2,\Delta;\tau_m)\exp(i2\pi\mathbf{q}_1\cdot\mathbf{R}_1) \times \exp(i2\pi\mathbf{q}_2\cdot\mathbf{R}_2)\mathrm{d}\mathbf{R}_1\mathrm{d}\mathbf{R}_2. \quad (13)$$

It is important to note that $\mathbf{q}_1$ and $\mathbf{q}_2$ may be varied independently or in unison. The former experiment (VEXSY [23]) is inherently two-dimensional and reveals the two-dimensional distribution function $\overline{P}_2(\mathbf{R}_1,\Delta;\mathbf{R}_2,\Delta;\tau_m)$. The latter experiment [double pulsed gradient spin echo (PGSE) NMR [19,20]] is inherently one-dimensional and reveals either the probability distribution of sum displacements (uncompensated case) or the probability distribution of difference displacements (compensated case). These one-dimensional experiments have been the subject of other studies [19,20,43,44]. In this paper we focus on the use of two-dimensional VEXSY.

The two-dimensional distribution function $\overline{P}_2(\mathbf{R}_1,\Delta;\mathbf{R}_2,\Delta;\tau_m)$ represents the two-time probability density of finding displacements $\mathbf{R}_1$ in the first and $\mathbf{R}_2$ in the second encoding interval of duration Δ, separated by a mixing time τ_m. If $\mathbf{q}_1$ and $\mathbf{q}_2$ are varied independently of each other, the function $\overline{P}_2(\mathbf{R}_1,\Delta;\mathbf{R}_2,\Delta;\tau_m)$ is obtained from the signal $E(\mathbf{q})$ after a double Fourier transformation with respect to $\mathbf{q}_1$ and $\mathbf{q}_2$. $\overline{P}_2(\mathbf{R}_1,\Delta;\mathbf{R}_2,\Delta;\tau_m)$ can be decomposed as

$$\overline{P}_2(\mathbf{R}_1,\Delta;\mathbf{R}_2,\Delta;\tau_m) = \overline{P}_1(\mathbf{R}_1,\Delta)\mathcal{P}_V(\mathbf{R}_1,\Delta|\mathbf{R}_2,\Delta;\tau_m), \quad (14)$$

where $\overline{P}_1(\mathbf{R}_1,\Delta)$ is the propagator during the first interval (which must be identical to the propagator in the second interval because of the time-invariance condition), and $\mathcal{P}_V(\mathbf{R}_1,\Delta|\mathbf{R}_2,\Delta;\tau_m)$ is the conditional probability that if a displacement by $\mathbf{R}_1$ occurs during the first interval Δ, then a displacement $\mathbf{R}_2$ will occur during the third time interval of equal duration to the first, delayed by a mixing time τ_m. This particular nomenclature has been chosen to emphasize that $\mathcal{P}_V$ describes the conditional probability between *displacements* in the VEXSY case, as compared to $P(\mathbf{r}_0|\mathbf{r}_1,t)$, which relates *positions* at times separated by *t*. The subscript *V* is used because displacement and velocity are simply related via the encoding time Δ. For convenience, we will abbreviate the function $\overline{P}_2(\mathbf{R}_1,\Delta;\mathbf{R}_2,\Delta;\tau_m)$ as $\overline{P}_2(\mathbf{R}_1,\mathbf{R}_2;\tau_m)$, where it is understood that the displacements $\mathbf{R}_1$, $\mathbf{R}_2$ are measured during two intervals each of duration Δ. A more detailed discussion of the formalism involved in the VEXSY experiment can be found in Ref. [25].

Note that unlike Eq. (12), which defines the one-dimensional propagator $\overline{P}_1(\mathbf{R},\Delta)$, Eq. (14) involves no integration, and, in consequence, the conditional probability can be obtained directly from a division of $\overline{P}_2(\mathbf{R}_1,\mathbf{R}_2;\tau_m)$ by $\overline{P}_1(\mathbf{R}_1,\Delta)$. It will be shown in the Results section that a plot of this conditional probability provides considerable insight into the correlation between velocities and can aid in the visualization of the relationships between initial and final velocity distributions.

It should be mentioned that, while the presentation of the results either as displacements or (via scaling with the encoding time Δ) as velocities is formally equivalent, some care has to be taken regarding the interpretation of the latter. If particle velocities fluctuate during Δ, either by contributions from random self-diffusion or dispersion due to the flow process itself, then the VEXSY experiment compares velocities that are already averaged over a finite time scale. The consequences of such averaging are discussed in Ref. [40]. For the purposes of the present work, the encoding times Δ have been chosen as short as practically possible.

DISPERSIVE LENGTH AND TIME SCALES RELEVANT TO THE NMR METHOD

In a two-dimensional exchange experiment, parameters measured at two different times separated by an exchange (or mixing) time are plotted in a two-dimensional graph. Diagonal intensity in such a graph represents spins whose parameters have remained unchanged over the mixing time, while off-diagonal intensity represents spins whose parameters have altered. It is of interest in the present context to understand how some simple limiting cases apply in the VEXSY experiment. In particular, we will consider the circumstances under which a purely diagonal spectrum might be obtained. In principle, we can always achieve this by setting the mixing time to zero. However, as discussed above, there does exist a finite encoding time Δ for the displacement in each interval. The limiting case of a diagonal spectrum requires not only $\tau_m \ll \tau_c$ but also $\Delta \ll \tau_c$. Here we discuss the feasibility of achieving such a limit.

Consider first the case of Brownian motion in the absence of flow. The Brownian correlation time (the molecular collision time) is much shorter than any encoding time Δ accessible by NMR, the latter being on the order of or greater than a few milliseconds. Thus the VEXSY spectrum compares two completely uncorrelated displacements and consists of the simple product of one-dimensional displacement distributions, a two-dimensional Gaussian. By contrast, consider the case of flow in a pipe involving a fluid. Here the molecular collision time remains as a fast correlation time but it is possible to imagine an experiment in which the displacements due to flow greatly exceed those due to Brownian motion. Now, however, molecules diffusing across streamlines leads to (Taylor) dispersion, for which the characteristic correlation time τ_c is the time to diffuse across the pipe, a^2/D_0, where a is the pipe diameter and D_0 is the molecular self-diffusion coefficient. This τ_c is on the order of hours for flowing water in capillaries of a few millimeters in diameter. It is therefore possible to perform an experiment in which the mixing time is much less than τ_c and for which the streamline displacements $v\Delta$ greatly exceed the Brownian displacements $(2D_0\Delta)^{1/2}$. Thus, a diagonal VEXSY plot is possible.

In porous media a much more subtle behavior applies. Let us once again allow that the mixing time is set to zero and that the condition for observing purely coherent flow is governed by the requirement $\Delta \ll \tau_c$, where now $\tau_c = d/\langle v \rangle$. In this limit we shall refer to the displacements $\langle v \rangle \Delta$ due to flow as Z_{flow}. This quantity can be made dimensionless in a number of ways. For the purposes of the present argument we shall find it convenient to do it in terms of the length scale $D_0\Delta/d$ as

$$\zeta_{\text{flow}} = Z_{\text{flow}} d/D_0\Delta \tag{15}$$

$$\approx \text{Pe} \tag{16}$$

The dispersive (incoherent) displacements are given by $[2D^*(\Delta)\Delta]^{1/2}$, where $D^*(\Delta)$ is the general time dependent dispersion (which at low Peclet number limit corresponds to molecular self-diffusion alone). Again, expressing the nondimensional dispersive displacement in terms of the length scale $D_0\Delta/d$, we find

$$\zeta_{\text{disp}} = [2D^*(\Delta)\Delta]^{1/2} d/D_0\Delta. \tag{17}$$

We now evaluate $D^*(\Delta)$. In doing so we choose to represent the universal asymptotic curve of Fig. 1 found from experiments on random bead packs by the relation

$$D^*(\infty) \approx D_0 + D_0 f(\text{Pe}), \tag{18}$$

where $f(\text{Pe})$ is dimensionless quantity on the order of Pe^{α}. Assuming for convenience the exponential form for the correlation function, we can thus write the time dependent dispersion as

$$D^*(\Delta) \approx D_0 + D_0 f(\text{Pe}\{1 + (\tau_c/\Delta)[\exp(-\Delta/\tau_c) - 1]\}. \tag{19}$$

Figure 3 compares the dimensionless flow displacement, dispersive displacement, and ratio τ_c/Δ as a function of Pe. Curves for two representative examples of diffusion coefficient and bead size relevant to our work are shown. The coherent and asymptotic regimes are indicated where the vertical line represents the $\Delta \sim \tau_c$ crossover at $\text{Pe} \sim d^2/D_0\Delta$. In the ''coherent'' regime where $\Delta \ll \tau_c$ we may evaluate Eq. (19) to second order to find

$$D^*(\Delta) \approx D_0[1 + f(\text{Pe})(\Delta/2\tau_c)]. \tag{20}$$

Given $\tau_c = d^2/\text{Pe}\, D_0$ and combining Eqs. (17) and (20), we find

$$\zeta_{\text{disp}} \approx [2(\tau_c/\Delta)\text{Pe} + \text{Pe}^{\alpha+1}]^{1/2}. \tag{21}$$

Within the range of Peclet numbers used in this study, $\alpha \geqslant 1$. Consequently the stochastic (dispersive) displacements always exceed the coherent (flow) displacements in the regime where coherent flow exists ($\tau_c/\Delta \gg 1$), irrespective of the parameters d, D_0, or Δ. For this reason a strongly diagonal VEXSY plot is not observable in the case of porous medium dispersion for the range of Peclet numbers used here ($\text{Pe} \leqslant 10^5$).

EXPERIMENTAL AND COMPUTATIONAL METHODS

The experiments were performed on fluid passing through a porous medium comprising randomly packed spherical beads. In separate experiments, three different sizes of beads were used, the respective diameters being 100, 400, and 500

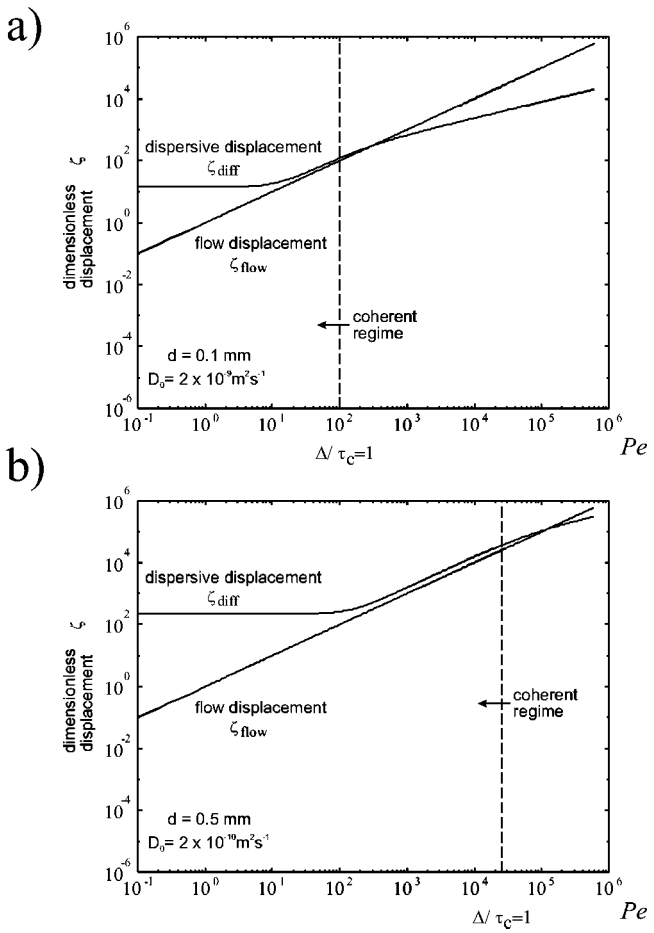

FIG. 3. Nondimensionalized displacements arising from flow and from dispersion versus Peclet number. Two examples are shown for bead sizes and molecular diffusion coefficients used in this work. To observe a diagonal VEXSY plot, complete coherence is required. This implies that both Δ and that steady state flow displacements exceed the stochastic dispersive displacements. The figure indicates that this condition is impossible to fulfill at Pe values used in this work.

μm. The 100- and 500-μm diameter beads were made from polystyrene and specified by the company (DUKE Scientific, Palo Alto, U.S.) to be monodisperse within a tolerance of 2.0%. Additional experiments were performed employing glass beads with a diameter of (400 ± 50) μm. Different containers were used for the differing bead sizes. For the 100-μm-diameter beads, a Teflon 2-mm-inner-diameter tube was used. To prevent a removal of the beads due to flow, two cotton wool plugs were instated at both ends of the packing. For the 400- and 500-μm diameter beads a poly(ether ether ketone) cylindrical container with an inner diameter of 10 mm and a length of 40 mm was used. In this latter arrangement, the sample was confined between plugs made from porous polystyrene. These plugs also acted as a diffusor, helping provide an even distribution of streamlines at the inlet and avoiding a holdup of fluid at the outflow. The porosities of the packings were determined to be 45% by weighting the sample before and after the addition of water. Samples were prepared by adding a mixture of liquid and beads to the liquid-filled container, the packing being regularly stirred to avoid trapping of air bubbles. Finally the containers were connected to a pump (Pharmacia 500, Pharmacia Biotech or BVP-Z, Ismatec) with a 2-mm-inner-diameter Teflon tube. To avoid pulsations of the liquid column, which can be introduced by the pump mechanism, a special gas reservoir was installed on the inlet part of the tube. This reservoir, which acted as a pressure buffer, was kept under nitrogen atmosphere to prevent dissolution of oxygen into the liquids.

Two different liquids were investigated, bidistilled water and a 70 wt. % solution of glycerol. These two liquids were chosen to have self-diffusion coefficients D_0 differing by one order of magnitude ($D_0=2.1\times10^{-9}$ m^2/s for water and 2.3×10^{-10} m^2/s for glycerol solution at room temperature). The liquids were pumped with various flow rates between 10 ml/h up to 10 l/h, corresponding to interstitial velocities ranging from 2 mm/s upto 20 mm/s for the 100-μm bead pack (small sample) and from 4 mm/s up to 80 mm/s for the 400- and 500-μm packs (large sample).

The NMR experiments were performed on an AMX 300-MHz Bruker spectrometer equipped with a vertical wide bore 7-T magnet. Two different gradient systems were used for the small and the large samples. For the larger sample a commercial Bruker gradient system with a maximum gradient strength of 1.6 T/m was employed. Experiments for the sample containing the smallest beads were performed with a homemade gradient system with 8 T/m gradient strength available.

One-dimensional pulsed gradient stimulated-echo (PGSTE) experiments were performed with the pulse sequence shown in Fig. 2(a). In order to allow for a wider range of encoding times Δ, the stimulated-echo method was used. In this method the magnetization is stored along the z direction (parallel to the main magnetic field component) between the second and third 90° pulses, where it is not subject to dephasing, and signal loss occurs due to longitudinal relaxation alone. The duration of the gradient pulses, δ, was typically 0.25 ms. For the two-dimensional VEXSY experiments, the stimulated-echo version of the pulse scheme has been used as well [see Fig. 2(c)] with similar gradient duration times δ and encoding times Δ chosen appropriately to provide a complete dephasing of the signal intensity at the highest gradient strength.

In order to simulate flow through a model porous medium, a packing of spherical particles of identical sizes was computer generated. This pack had a porosity of 44%, consisting of N_C^3 elementary cubes with $N_C=64$, where the bead diameter was chosen as 300 μm. Both porosity and sphere size were matched to real samples of glass bead packings for which experiments with water flow had been performed previously [24,45,46]. Their properties match those of the samples used in the experimental part of this study reasonably well. To generate an adequate representation of the real porous medium, the random sphere packing has been simulated by successive deposition of grains in a ''gravitational'' field. The Nth grain is introduced at a random location above the bed of $N-1$ grains already deposited and is allowed to fall until it reaches a local minimum of its potential energy. The matrix possessed periodic boundary conditions. A more

detailed description of the deposition process is found in Ref. [47].

In the following step, the three-dimensional velocity field was computed for each position in the pore matrix. For an incompressible Newtonian fluid at low Reynolds numbers, flow is governed by the usual Stokes equations

$$\nabla p = \mu \nabla^2 \mathbf{v}, \quad \nabla \cdot \mathbf{v} = 0, \tag{22}$$

where $\mathbf{v}$, p, and μ are the velocity, pressure, and viscosity of the fluid, respectively, and $\mathbf{v}=\mathbf{0}$ on the surface of the wetted solid. The symmetric permeability tensor $\mathbf{K}$ only depends on the geometry of the system and describes the relation between the macroscopic pressure gradient $\overline{\nabla p}$ and the seepage velocity $\langle v \rangle$:

$$\langle v \rangle = -\frac{1}{\mu} \mathbf{K} \overline{\nabla p}. \tag{23}$$

The numerical method used to solve these equations is outlined in Ref. [48]. It assumes low Reynolds numbers which are guaranteed by the conditions employed in this study: the flow field was computed for average velocities of 2.35 and 4.7 mm/s, respectively, corresponding to Re=0.7 and 1.4. More important, however, is the relative weight of convective and diffusive displacements to the total particle motion, which is expressed by the dimensionless Peclet number [see Eq. (5)]. It was shown [35] that these simulations were reliable for Peclet numbers smaller than 1000. In the case given above, one computes Pe=270 and 540.

In the final step, 100 000 particles were distributed evenly in the pore space and were allowed to follow the flow lines and undergo random self-diffusion jumps, where wall collisions were taken into account by accumulating individual time lags to each particle, which were then recovered at regular intervals. The displacements Z parallel to the main flow direction were saved periodically and served for the visualization of the two-dimensional (2D) probability functions and the computation of the correlation coefficients.

The simulation methods have been discussed in greater detail and compared to experimentally obtained propagators in [45,49]. A similar set of simulated data for flow through bead packings, in particular, addressing the topic of spatial correlations between displacements in orthogonal directions at identical times, was already presented in previous work [24,45]. The results from numerical simulations, which are presented in this work with the purpose of supplying a comparison with experimental data, will be covered more extensively in Ref. [40].

RESULTS AND DISCUSSION

One-dimensional propagators

In the idealized case, the VEXSY experiment compares velocity distribution functions which were obtained at two different time points. In reality, the encoding takes place over an interval Δ during which a certain averaging of particle velocities occurs. The desired time scale is determined by two limiting conditions. First, we wish to make Δ long enough that the influence of microscopic Brownian motion is minimized. To ensure that the displacement due to flow dominates the rms displacement due to Brownian motion, we require

$$\langle v \rangle \Delta \gg \sqrt{2 D_0 \Delta} \quad \text{or} \quad \Delta \gg \frac{2 D_0}{\langle v \rangle^2}. \tag{24}$$

For the smallest average velocities used in this study, 3 mm/s, this condition puts a lower limit of $\approx$1 ms for the encoding time Δ. Higher velocities allow still smaller encoding times if we are to meet this condition. On the other hand, the maximum gradient strength available makes Δ values of less than 1 ms unfeasible, so that the above condition for the lower limit of Δ is fulfilled under all circumstances reported here.

Second, we wish to make Δ short enough that the flow velocity is approximately constant over the encoding time. This allows us to use the *exchange time* between the two encodings, τ_m, to investigate velocity fluctuations. This condition implies that the encoding time be much less than the correlation time, $\Delta \ll \tau_c$.

In order to demonstrate the influence of different Δ on the shape of the velocity distribution function, we present as an example in Fig. 4 a series of one-dimensional propagators $\overline{P}_1(Z,\Delta)$, where Z indicates displacements along the axis of the main flow direction, being encoded by a pulsed gradient in the same direction, whose corresponding wave number we denote as q_z. The propagators were obtained employing the conventional PGSTE pulse sequence shown in Fig. 2(a). Figure 4 was obtained with beads of 500 μm diameter at a volume flow rate of 3.0 l/h, corresponding to an average velocity of 24 mm/s and Pe=5600. The correlation time under these conditions is $\tau_c=21$ ms. The velocity distribution function, which is equivalent to the propagator of displacements ($Z=v\Delta$), shows a sharp peak at small velocities and a long tail of large velocities for the shortest encoding time of

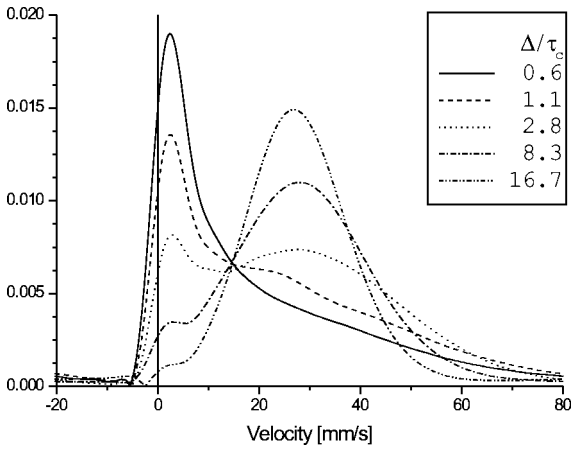

FIG. 4. One-dimensional propagators $\overline{P}_1(Z,\Delta)$ for flow of water in packed beads of 500 μm diameter at a volume flow rate of 3.0 l/h, corresponding to an average velocity of 24 mm/s, $\tau_c=21$ ms, and Pe=5600. The propagators were obtained with encoding times Δ varied as indicated, employing the double-PGSE pulse sequence shown in Fig. 3(a).

$\Delta = 10$ ms. This behavior has been observed before [50–52] and has been well represented by an exponentially decaying velocity distribution function. It describes a situation where each particle remains essentially within the same streamline during the encoding ($\Delta < \tau_c$), so that the statistics of displacements of the ensemble of flowing molecules can be regarded as being equivalent to the true properties of the velocity field.

With increasing encoding time, the particles mix between streamlines, this mixing process being dominated by the influence of mechanical dispersion. As a consequence of this mixing, the velocity distribution function of the particles becomes smoothed over the interval Δ. The effect of this averaging process is already visible for $\Delta/\tau_c = 1.1$. For $\Delta \gg \tau_c$, the distribution is approximately Gaussian and is centered at the average interstitial velocity, $\langle v \rangle = 28$ mm/s. A small ''hump'' representing ''slow'' spins remains even at $\Delta = 300$ ms. The origin of this hump is a small fraction of molecules, which remains trapped in quasistatic regions without having mixed into the main streamlines during Δ. This behavior is in perfect agreement with propagators reported in the literature [53–55], and is reasonably well understood. In the limit $\Delta \to \infty$, the propagator is expected to be of perfect Gaussian shape, representing the case when each spin has sampled all velocities with an equal statistical probability irrespective of its starting position or initial velocity. This is the asymptotic region of longitudinal dispersion [56–58]. It has been shown that the intensity of the low-velocity peak as a function of Δ is a measure of the connectivity of the pore space [6,52,59], and it has been observed for times much exceeding $\Delta = \tau_c$ for systems with low porosity and connectivity [46].

In order to compare the instantaneous velocity distributions at two different times, it becomes obvious from the results of Fig. 4 that the encoding time Δ has to be chosen as short as possible, provided of course that $\Delta \langle v \rangle \gg (2D_0\Delta)^{1/2}$ is still fulfilled.

One way to indirectly observe the change of velocities during a given period is realized by a repeated encoding of displacements in two identical intervals Δ, which are separated by a mixing time τ_m. This is essentially a one-dimensional realization of the VEXSY experiment [see Figs. 2(b) and 2(c)], where both gradient pairs are varied simultaneously. Two versions are possible, one in which the gradient pairs have the same effective amplitude (uncompensated double PGSE) and one in which the gradient pairs have the opposite effective amplitude (compensated double PGSE). On Fourier transformation of this doubly encoded signal with respect to the wave vector q_z, the former returns the total displacement from each interval Δ, from which the average velocity distribution may be computed, while the latter yields the difference in displacement from each interval. Figure 5 shows the distribution of average velocities obtained using gradients of the same effective amplitude (uncompensated double PGSE for a range of mixing times, τ_m). For a vanishing mixing time, this function is essentially unchanged compared to the single-encoding case shown in Fig. 4. With the chosen parameter of $\Delta = 5$ ms for the uncompensated double-PGSE experiment, the result is equivalent to the single-PGSE experiment with a twice larger encoding time of $\Delta = 10$ ms. The effective time over which velocity changes are measured is denoted by $\tau_m' = \Delta + \tau_m$, and the reduced quantity τ_m'/τ_c is used as a parameter in this and the following figures.

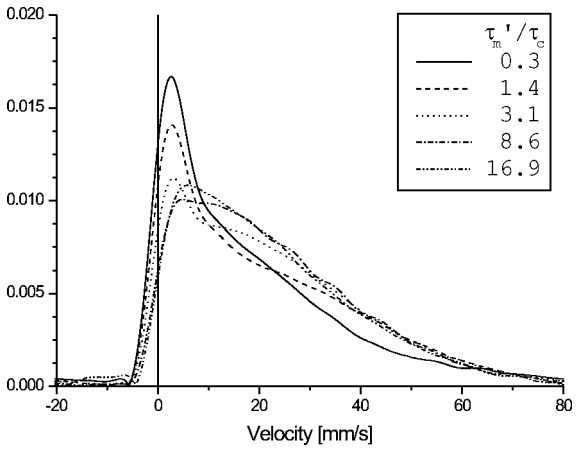

FIG. 5. One-dimensional propagators $\overline{P}_1(Z,\Delta)$ for flow of water in packed beads of 500 μm diameter at a volume flow rate of 3.0 l/h, corresponding to an average velocity of 24 mm/s, $\tau_c = 21$ ms, and Pe = 5600. The propagators were obtained with an encoding time of $\Delta = 5$ ms employing the double-PGSE pulse sequence shown in Fig. 3(c). The mixing time τ_m has been varied as indicated.

As τ_m' increases, the velocities of the individual fluid elements during the first and second encoding interval become more and more uncorrelated. In the limit of infinite τ_m', the signal function can be split into a product of two individual propagators:

$$E(q_z) = \int\int \overline{P}_2(Z_1, Z_2; \tau_m') \exp[i2\pi q_z (Z_1 + Z_2)] \mathrm{d}Z_1 \mathrm{d}Z_2$$
$$= \left[\int \overline{P}_1(Z,\Delta) \exp(i2\pi q_z Z) \mathrm{d}Z \right]^2, \qquad (25)$$

so that the Fourier transformation of $E(q_z)$ with respect to q_z produces the autocorrelation function of the one-dimensional propagator $\overline{P}_1(Z,\Delta)$.

This one-dimensional double-PGSE experiment is shown for demonstration only. It does not give direct insight into the change of velocities, neither does it allow one to investigate the behavior of particular subsets of fluid elements in sufficient detail. By contrast, the use of the compensated double-PGSE experiment does reveal changes in velocity, and such an approach has been employed in previous work [19,20]. However, the use of the two-dimensional VEXSY experiment allows a more detailed analysis of the changes in the velocity field in which specific correlations in displacements between the two encoding intervals are revealed.

Characteristics of VEXSY propagators

Figure 6(a) demonstrates the evolution of the two-time joint probability density of velocities, $\overline{P}_2(Z_1, Z_2; \tau_m')$. This

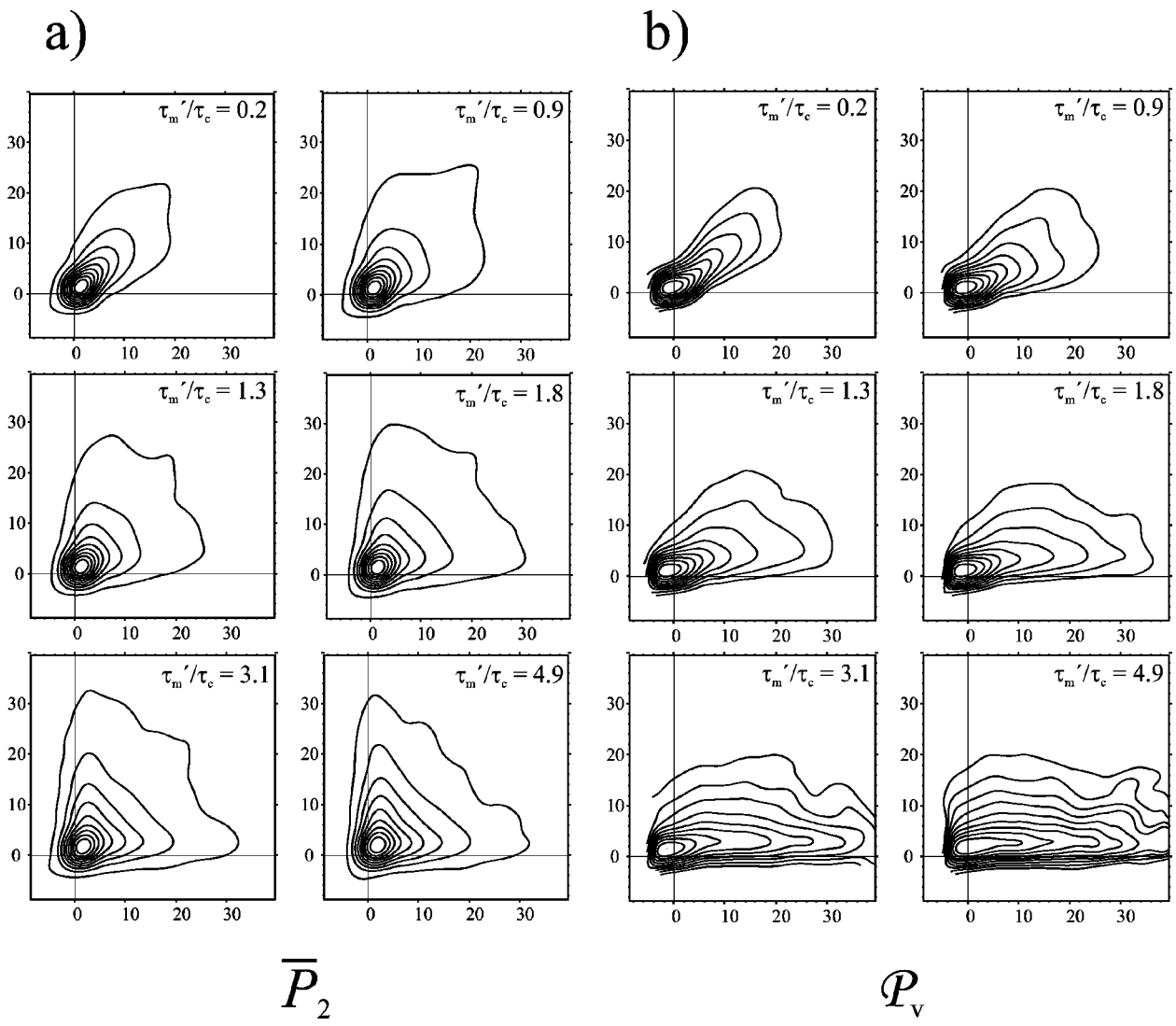

FIG. 6. (a) Two-time joint probability density of velocities, $\overline{P}_2(Z_1,Z_2;\tau_m)$, for water flowing through packed beads of 500 μm diameter obtained by the VEXSY experiment as shown in Fig. 3(c). The parameters of the experiments were flow rate $Q=1.0$ l/h, average velocity $\langle v\rangle=7.9$ mm/s, corresponding to $\tau_c=64$ ms and Pe$=1900$; the encoding time is $\Delta=12$ ms. Velocities measured before and after the mixing interval τ_m are shown along the abscissa and ordinate axes, respectively. Numbers indicate velocities in mm/s. Contour lines are in steps of 10% where the peak amplitude is normalized to unity. (b) As in Fig. 6(a) but with the data plotted as the conditional probability $\mathcal{P}_V(Z_1,\Delta|Z_2,\Delta;\tau_m)$.

plot was obtained by using the VEXSY experiment as shown in Figs. 2(b) and 2(c) in which the amplitudes of both gradient pairs were varied independently of each other, following which the signal was subjected to a two-dimensional Fourier transformation with respect to $\{q_{z1},q_{z2}\}$. Here and in all following experiments, only displacements parallel to the axial flow direction (Z) have been measured. The parameters of the experiments were the flow rate $Q=1.0$ l/h, average velocity $\langle v\rangle=7.9$ mm/s, bead size $d=500$ μm, corresponding to Pe$=1900$. The correlation time computed for these conditions is $\tau_c=64$ ms. The mixing times used in the experiment cover the range $\tau_m'\ll\tau_c$ to $\tau_m'\gg\tau_c$. Note that in this and all subsequent plots the ordinate and abscissa axes are in velocity rather than displacement units. Conversion between displacement and velocity may be simply made via the encoding time Δ.

For a negligible mixing time, the velocity distribution is expected not to change between the first and the second encoding interval. The plot in the upper left corner of Fig. 6(a) shows this situation for $\tau_m'=13$ ms. The distribution is plotted with initial velocities along the horizontal axis, and final velocities along the vertical. Intensities along the main diagonal correspond to spins that have not changed their velocity during τ_m', while off-diagonal intensities represent velocity changes. Here and in all following figures, the two-time probability density function $\overline{P}_2(Z_1,Z_2;\tau_m')$ is plotted as contour lines in steps of 10% where the peak amplitude is normalized to unity. The plot for the shortest mixing times is characterized by a strong alignment along the main diagonal, indicating that the majority of spins have maintained their initial velocity or have changed it by a relatively small amount. In fact, the broadening of the distribution function is

dominated by the averaging process taking place during Δ because $\Delta > \tau_m'$. As explained in the preceding section, a perfectly diagonal VEXSY plot is not observable in flow through bead packs for the range of Peclet numbers used in this work. The function $\overline{P}_2(Z_1,Z_2;\tau_m')$ therefore does not assume the shape of a δ distribution as would be expected for a vanishing mixing time, but retains a finite broadening which represents the highest degree of correlation obtainable.

When τ_m' is increased, a further broadening of the function $\overline{P}_2(Z_1,Z_2;\Delta)$ is observed. The probability of a change of velocities for a given fluid element grows with longer τ_m'. In the third frame, $\tau_m' \sim \tau_c$ and one finds a larger probability of velocity changes. For example, the probability of finding a spin with a large velocity in the first encoding interval *and* a small velocity in the second interval is increased as compared to the situation in the first frame. The loss of correlation, however, is not yet complete at $\tau_m' \sim \tau_c$. At long τ_m' the shape of the function $\overline{P}_2(Z_1,Z_2;\tau_m')$ tends to become triangular, with the outer contour lines being oriented parallel to the secondary diagonal in the plot. The latter effect suggests a constant probability of finding spins with equal average velocity, equivalent to a constant total displacement during both intervals, Z_1+Z_2. This requires a negative correlation between displacements Z_1 and Z_2 at least for those particles that have traveled the longest accumulated distances. In other words there is a tendency for a small Z_1 to be observed along with a large Z_2, and vice versa, a strange result given that one would expect a complete loss of correlation for mixing times much longer than the correlation time. This apparently unphysical observation could arise from inflow/outflow effects as discussed further in the Appendix.

The interpretation of the dependence between initial and final velocity distributions can be facilitated by employing the conditional probability $\mathcal{P}_V(Z_1,\Delta|Z_2,\Delta;\tau_m')$ as defined in Eq. (14). It is simply obtained in practice by dividing the joint probability density function $\overline{P}_2(Z_1,Z_2;\tau_m')$ by the one-time propagator $\overline{P}_1(Z,\Delta)$, which is the marginal of $\overline{P}_2(Z_1,Z_2;\tau_m')$, i.e., the integral $\int \overline{P}_2(Z_1,Z_2;\tau_m')dZ_2$. $\mathcal{P}_V(Z_1,\Delta|Z_2,\Delta;\tau_m')$ is still a two-dimensional quantity, and the plots obtained from the VEXSY results of Fig. 6(a) are shown in Fig. 6(b). The shape of the conditional probability describes the probability of finding a velocity v_2 in the second encoding interval *given that* a velocity v_1 was observed in the first interval. It can be seen that for the shortest mixing time, a strong correlation between v_1 and v_2 exists, as expressed by the probability of finding v_2 being shifted towards higher velocities at increasing v_1. Throughout the function, a positive slope of around unity is found, i.e., the pattern of contour lines is aligned approximately along the main diagonal. Note that for $v_1 = 0$, the distribution of v_2 remains very narrow and is centered about a small positive value, as a change of velocities will most likely be associated with a positive (''downstream'') motion of the fluid elements. This is corroborated by the one-dimensional propagators shown in Fig. 4, where negative displacements, arising from the combined effect of backflow and random diffusive contributions antiparallel to the main axial flow direction, remain very small.

With growing mixing time, the fluid elements are allowed to sample a wider range of streamlines and the different components of dispersion lead to a loss of memory, so that the conditional probability of v_2 becomes gradually less dependent on the initial value v_1. The alignment of contour lines changes from the main diagonal toward a flatter slope considerably less than unity. The slope, however, does not remain uniform for all values of v_1, a feature which becomes more obvious at higher Peclet numbers and which will be discussed in the following sections. As the mixing time τ_m' exceeds the correlation time τ_c, the contour lines tend to become oriented parallel to the horizontal (v_1) axis. This behavior is equivalent to the conditional probability of v_2, becoming independent of v_1, so that the correlation is being lost. However, for the longest time shown in Fig. 6(b) ($\tau_m' \sim 5\tau_c$), this limit of total correlation loss is not yet quite reached. A small positive slope remains visible for small v_1, while a parallel alignment of the contour lines is mainly observed for small and negative v_2. A slightly negative slope is observed for the combinations of both large v_1 and v_2. This latter behavior may be due to the influence of the outflow effect described in the Appendix; contour lines of $\overline{P}_2(Z_1,Z_2;\tau_m')$ parallel to the secondary diagonal of constant average velocity correspond to a negative correlation between large values of v_1 and v_2 in $\mathcal{P}_V(Z_1,\Delta|Z_2,\Delta;\tau_m')$.

Dependence of VEXSY propagators on the Peclet number

In Figs. 6–8, 10, and 11, we present experimental results obtained by VEXSY along with plots of the conditional probabilities for a wide range of mixing times and Peclet numbers. This evolution encompasses the shortest to the longest mixing times that could be used under the experimental conditions. Three orders of magnitude of Peclet numbers are covered. Full experimental parameters for flow rate, average velocity, encoding time, and correlation time are given in the figure captions.

In order to further interpret the experimental data we will begin with providing a comparison of experimentally obtained VEXSY functions (Fig. 8) with those obtained from numerical simulations, under similar conditions (Fig. 9). The numerical procedure has been described before and has been proven to give results in good agreement with the NMR experiments for a variety of different problems, such as one-dimensional propagators for flow in porous media [49] as well as spatially two-dimensional propagators comparing displacements in orthogonal directions [45,46]. The main deviation of the simulations was found in a prolonged persistence of the low-velocity peak and in a somewhat limited resolution of the model matrix [45,49], while computations of the general statistical behavior of the flow field were shown to be reliable.

In the work presented here, we compare experimental data and simulations under similar nondimensional conditions, i.e., similar Peclet numbers and τ_m'/τ_c values, although the absolute values of flow parameters do not precisely correspond. Figure 8 presents experiments obtained with an en-

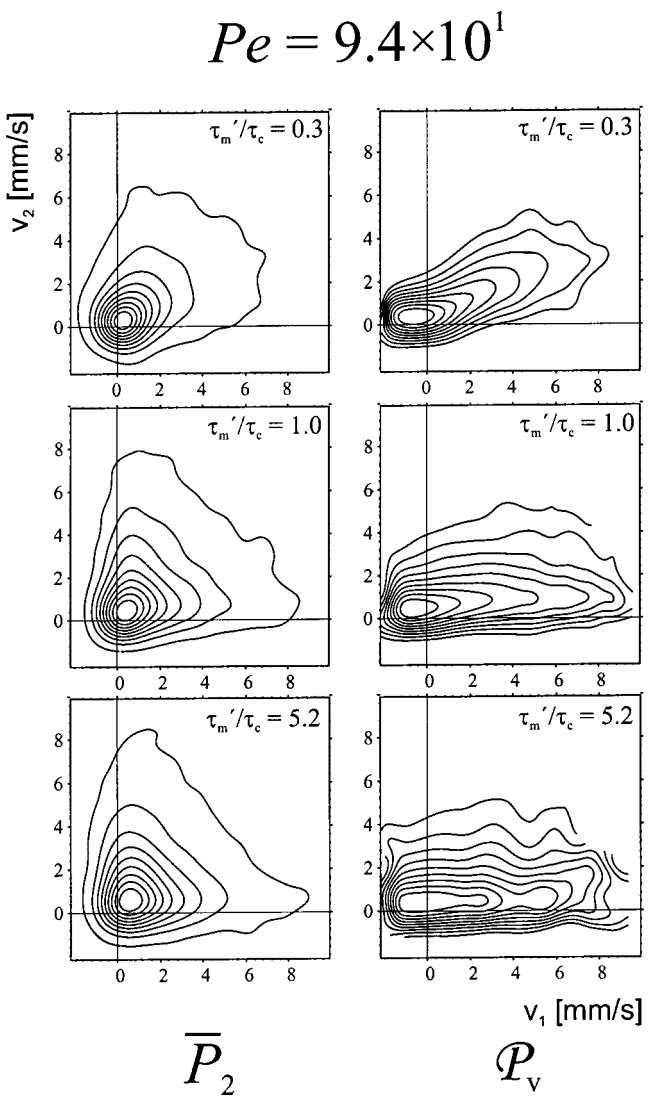

FIG. 7. Two-time joint probability density of velocities, $\overline{P}_2(Z_1,Z_2;\tau_m)$ (left-hand side), and conditional probability $\mathcal{P}_V(Z_1,\Delta|Z_2,\Delta;\tau_m)$ (right-hand side) for water flowing through packed beads of 100 μm diameter. The parameters of the experiments were flow rate $Q=10$ ml/h, average velocity $\langle v\rangle = 2.0$ mm/s, corresponding to Pe=94; the encoding time is $\Delta = 12.5$ ms. $\tau_c = 51$ ms. Contour lines are in steps of 10% where the peak amplitude is normalized to unity.

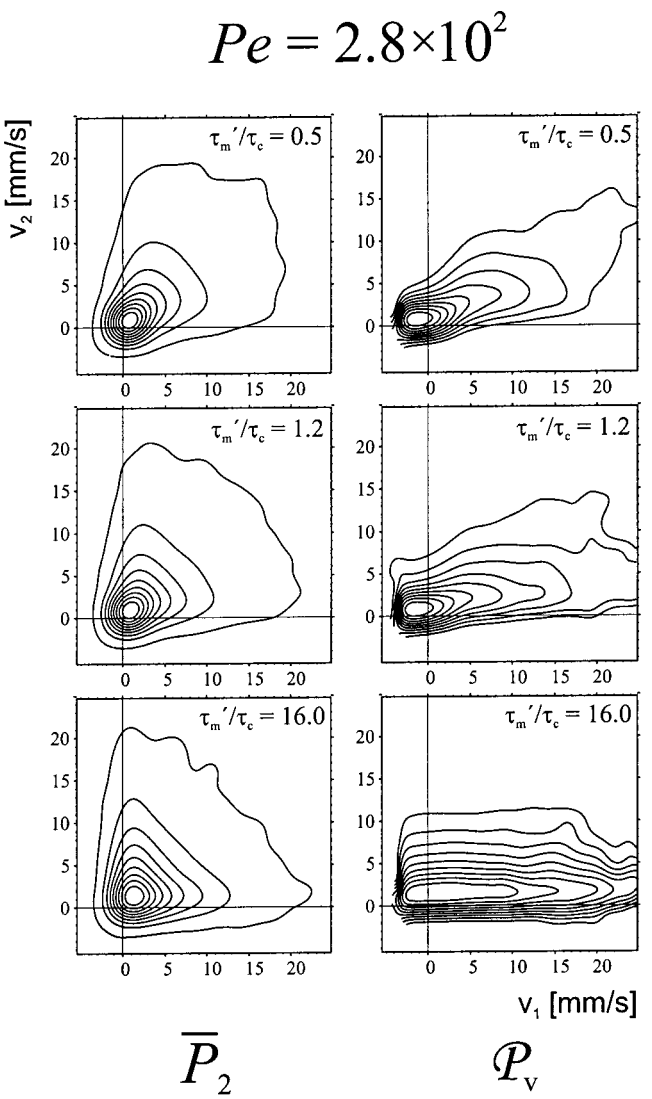

FIG. 8. Two-time joint probability density of velocities, $\overline{P}_2(Z_1,Z_2;\tau_m)$ (left-hand side), and conditional probability $\mathcal{P}_V(Z_1,\Delta|Z_2,\Delta;\tau_m)$ (right-hand side) for water flowing through packed beads of 100 μm diameter. The parameters of the experiments were flow rate $Q=30$ ml/h, average velocity $\langle v\rangle = 5.9$ mm/s, corresponding to Pe=280; the encoding time is $\Delta = 5$ ms. $\tau_c = 17$ ms. Contour lines are in steps of 10% where the peak amplitude is normalized to unity.

coding time of $\Delta=5$ ms for a bead size of 100 μm at a volume flow rate of 30 ml/h, corresponding to an average velocity of 5.9 mm/s, $\tau_c=12.5$ ms, and Pe=280. The simulations shown in Fig. 9 were obtained for a reconstructed random bead packing for Pe=270. Because of a different choice of the self-diffusion coefficient and encoding time, leading to a somewhat different ratio of the contribution of Brownian motion, $(2D_0\Delta)^{1/2}$, to the displacement during the encoding time, $\langle v\rangle\Delta$, the velocity distribution function is slightly broader in the case of the simulation.

A common feature across both experiment and simulation is the gradual change from a preferential alignment of the contour lines along the main diagonal in the VEXSY plot (left-hand columns of Figs. 8 and 9) for short mixing times towards a roughly triangular shape as τ_m' increases. A common feature of both series of plots is the tendency of the alignment of the outer contour lines (representing low probability) along the secondary diagonal. It is clear that while some of the apparent negative correlation in the experimental data may be attributed to the inflow/outflow effect, some must arise from dispersive fluctuations themselves, since a similar tendency, albeit weaker, is seen in the simulations, which were performed without taking the finite length of the measuring volume into account. Correspondingly, the contour lines in the plots of the conditional probability (right-hand columns) become perfectly parallel to the horizontal axis, and a similar behavior is seen for the experimental data in the lower frame, where $\tau_m' \sim 16\tau_c$.

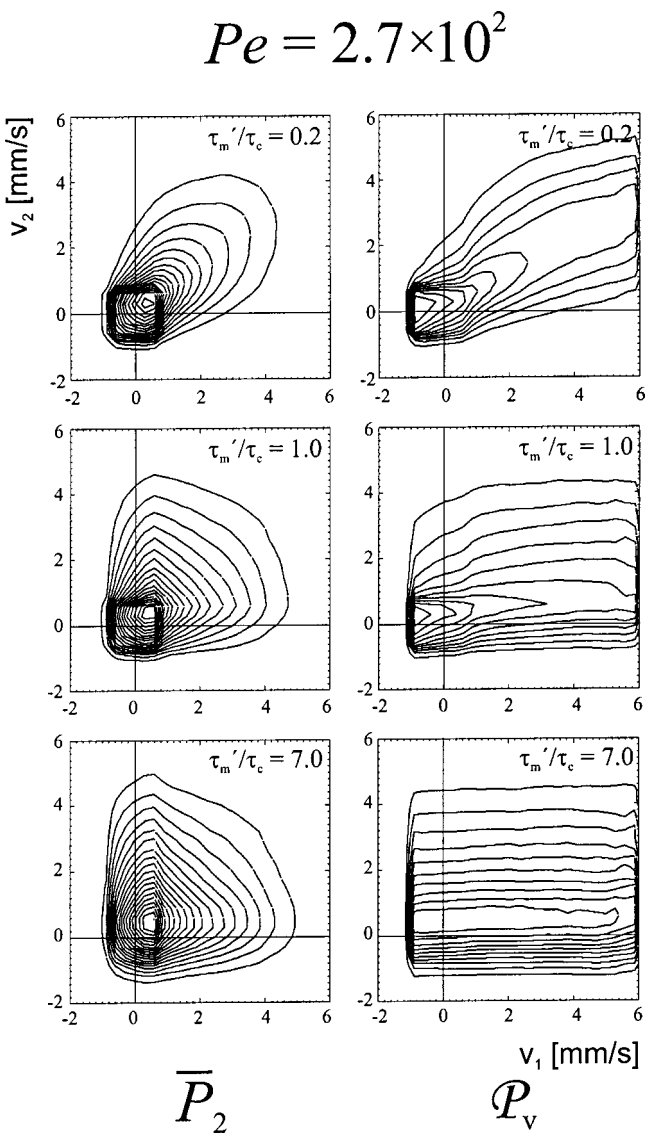

FIG. 9. As in Fig. 8, but numerical simulations for water flowing through a randomly generated bead pack with Pe=270.

Even for the smallest Peclet number of 94 (Fig. 7), the contributions of random motions due to Brownian self-diffusion are outweighed by the coherent motions of flow itself. Nevertheless, for the reasons described earlier, one observes a considerable broadening of the joint probability density $\bar{P}_2(Z_1,Z_2;\tau_m')$ for vanishing mixing time τ_m'. As in all other experiments, the encoding time Δ for the determination of velocities has been kept as small as possible. However, in order to allow the measurement of the complete propagator for the relatively slow average velocity of 2.0 mm/s, an encoding time of $\Delta=12.5$ ms had to be used. This corresponds to an rms Brownian displacement of 8 μm and an average displacement due to flow of 25 μm. The contribution of random Brownian motion is thus not negligible, and the broadening of the propagator is essentially determined by the velocity fluctuations during Δ in the first and the second encoding interval. While a strong positive correlation between displacements during the two intervals is clearly seen from the conditional probability plot on the right-hand side, it is not aligned along the main diagonal, indicating a degree of reduction in correlation. In the middle pair of frames, the effective mixing time τ_m'—representing the time between the centers of each encoding interval—is equal to τ_c. One observes a considerably broadened, rounded triangular shape of the joint probability function with a flattening towards large average velocities. The decay of the probability density is much less steep than in the higher Peclet number plots shown in Figs. 6, 8, and 9, i.e., the peak around small displacements is much less pronounced. This observation is consistent with the one-dimensional measurements in which we observed a more efficient mixing of quasistatic pools of fluid into the flowing medium at lower Peclet numbers. The plot of the conditional probability shows a weakly pronounced positive correlation at the shortest mixing time, while at $\tau_m'=263$ ms$\sim 5.2\tau_c$, such a correlation cannot be discerned anymore. The shape of $\bar{P}_2(Z_1,Z_2;\tau_m')$, on the other hand, changes imperceptibly from $\tau_m'=52.5$ ms to $\tau_m'=263$ ms. Even for this long mixing time, the outflow effect can be regarded as negligible as the displacement of the fastest fluid elements is still much smaller than the size of the resonator.

Figure 10 shows the results of experiments obtained at similar mixing times, but at an even higher Peclet number of 8600. The experiments have been performed on a water-glycerol mixture with a relatively long encoding time of $\Delta=35$ ms, which, due to the smaller self-diffusion coefficient of the fluid, corresponds to an rms displacement of only 4 μm compared to $\langle v\rangle\Delta=137$ μm. The upper frames exhibit a much stronger correlation than that seen at lower Peclet numbers, this correlation being indicated by the narrow ridge of $\bar{P}_2(Z_1,Z_2;\tau_m')$ along the main diagonal, surrounded by a broader ''halo'' of the lowest contour lines representing the fraction of fastest fluid elements. This halo continues to broaden with increasing mixing time, while the contour lines of highest intensity, produced by the large fraction of slower spins, take longer to change their shape. Again, the center frame corresponds to the situation where $\tau_m'\sim\tau_c=127$ ms. A direct comparison between the center frames of Figs. 7 and 10 reveals an important difference. For the larger Peclet number, the correlation between initial and final velocities seems to be much more persistent. This stands in contrast with the predictions of the simplified model of the Ornstein-Uhlenbeck type [see Eq. (7)] in which the decay of the velocity autocorrelation function would be given by a single characteristic time τ_c. The plot of Fig. 10 gives a strong indication that this assumption is not suitable when describing the details of the temporal correlations of the flow process.

The information obtained from the NMR experiments employing the VEXSY scheme allows for distinction between different subsets of fluid elements. For example, the different behaviors of the contour lines of the joint probability function $\bar{P}_2(Z_1,Z_2;\tau_m')$ (left-hand side of Fig. 10) for slow and fast particles makes it necessary to discuss them separately from each other. This is facilitated by taking the shape of the conditional probability $\mathcal{P}_V(Z_1,\Delta|Z_2,\Delta;\tau_m')$ (right-hand side

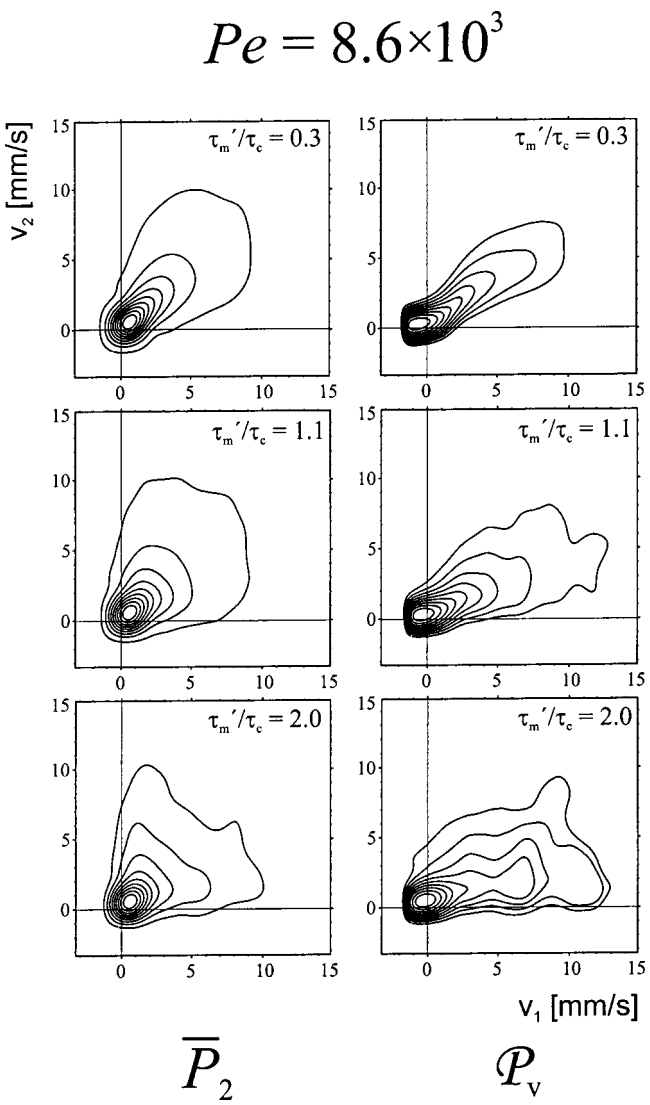

FIG. 10. As in Fig. 8, but for a water-glycerol mixture flowing through packed beads of 500 μm diameter. The parameters of the experiments were flow rate $Q=0.5$ l/h, average velocity $\langle v\rangle = 3.9$ mm/s, corresponding to Pe=8600; the encoding time is $\Delta = 35$ ms. $\tau_c = 127$ ms. Contour lines are in steps of 10% where the peak amplitude is normalized to unity.

of Fig. 10) into account. A sigmoidal shape can be clearly discerned in the upper two frames, an effect that is also apparent, albeit less pronounced, in various other plots for smaller Peclet numbers. The shape of $\mathcal{P}_V(Z_1,\Delta|Z_2,\Delta;\tau_m')$ can be separated into three regions. For small velocities, the contour lines lie horizontally, i.e., the conditional probability of finding a particular velocity after the mixing time is independent of the value before the mixing time. This accounts for spins which reside in quasistatic pools for which flow slowly so that their displacements are essentially dominated by the contributions of random self-diffusion. For intermediate velocities, a strong correlation is found. This subset of spins follows streamlines but have not yet encountered geometrical obstacles which can lead to mechanical dispersion and therefore to a change of velocities. The fastest particles, however, have traveled distances comparable to the structural size of the system, in our case the bead size, and have changed their direction and/or magnitude of velocity. For example, the subensemble of spins possessing velocities of 10 mm/s in Fig. 10 have traveled distances of 0.36, 1.35, and 2.55 mm, respectively, at the three shown mixing times, τ_m', which compares to the bead size of 0.5 mm.

The time it takes for an individual particle to travel a distance d obviously depends on its local velocity. The distribution of local flow velocities can thus be tentatively translated into a distribution of individual correlation times, $P(\tau_c)$. It must be understood that this distribution only serves as a means of interpretation and, like the propagator $\overline{P}_1(Z,\Delta)$, depends on the time scale over which the measurements are taken. However, the two-dimensional NMR technique of VEXSY provides a unique method of distinguishing and quantifying the behavior of individual subsets of the moving fluid.

The experimental results for the highest Peclet number, Pe=86 000 (see Fig. 11), follow a pattern similar to that described above. The distinction between fast and slow fluid elements becomes even more pronounced than for Pe =8600. The halo of fast spins (outer contour lines) loses correlation before the slow spins (inner contour lines). This effect is clearly observed for the two shorter mixing times where $\tau_m' \ll \tau_c$ (upper pair of frames) and $\tau_m' \sim \tau_c$ (central pair of frames). However, even for the longest mixing time ($\tau_m' \sim 5\tau_c$) a correlation between velocities still exists for the slowest particles which have traveled distances smaller than the bead size. Nonetheless, the sigmoidal shape of the conditional probability is observed for the two shorter mixing times.

We now investigate the importance of the Peclet number for the loss of temporal correlations of velocities. Here we directly compare results obtained with comparable reduced mixing times (on the order of $\tau_m' \sim \tau_c$) for different Peclet numbers. The results are summarized in Fig. 12. From top to bottom, the values of τ_m' correspond to between 1.0 and 1.1 times the correlation time τ_c, respectively, the latter being computed using the bead diameter as a reference length scale of the system. Assuming a simple Ornstein-Uhlenbeck process with a single correlation time, a similar behavior would be expected in each case. The changing shape of both the joint two-time probability density function $\overline{P}_2(Z_1,Z_2;\tau_m')$ and the conditional probability $\mathcal{P}_V(Z_1,\Delta|Z_2,\Delta;\tau_m')$ with increasing Peclet number clearly indicates that a distribution of correlation times has to be taken into account, and that this distribution $P(\tau_c)$ may itself depend on Pe, much like that observed for the one-dimensional propagator $\overline{P}_1(Z,\Delta)$.

On the left-hand side of Fig. 12, it becomes obvious that the peak related to slow moving fluid elements is more pronounced for high Peclet numbers, where the total fluid transport is mainly determined by a relatively small fraction of spins with a high velocity. As a consequence, the difference between slow and fast particles becomes more pronounced as Pe increases. The conditional probability plots on the right-hand side of Fig. 12 are more instructive. At the lowest value, Pe=94, the conditional probability exhibits little structure, while at higher values of Pe, the sigmoidal shape

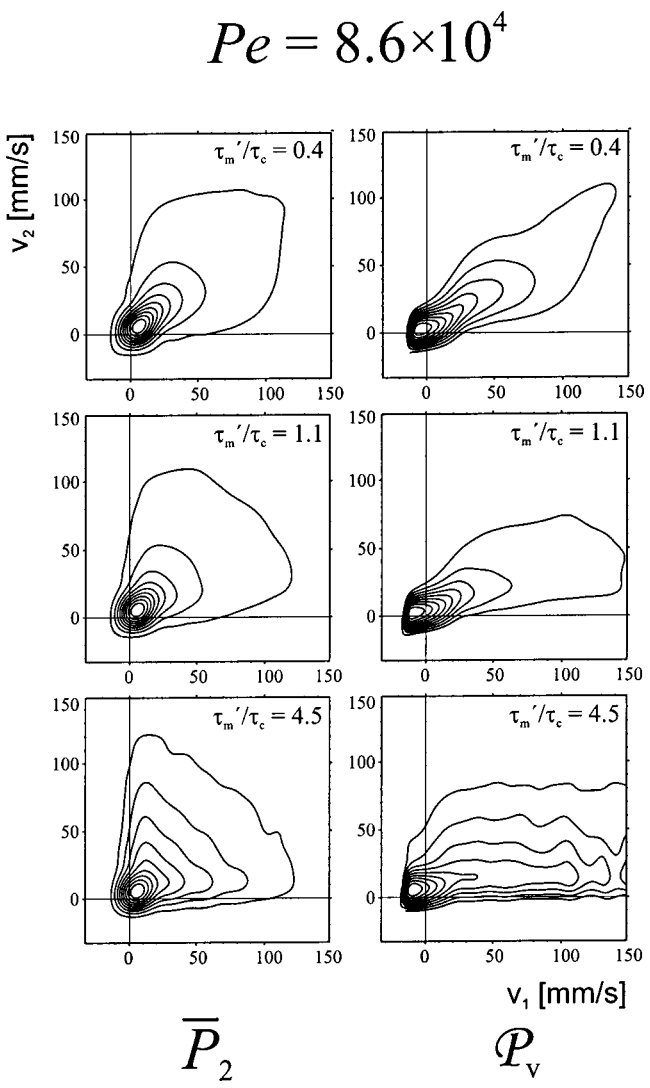

FIG. 11. As in Fig. 10, but with the following experimental parameters: flow rate $Q=5.0$ l/h average velocity $\langle v\rangle=39$ mm/s, corresponding to Pe=86 000; the encoding time is $\Delta=3.5$ ms. $\tau_c=13$ ms. Contour lines are in steps of 10% where the peak amplitude is normalized to unity.

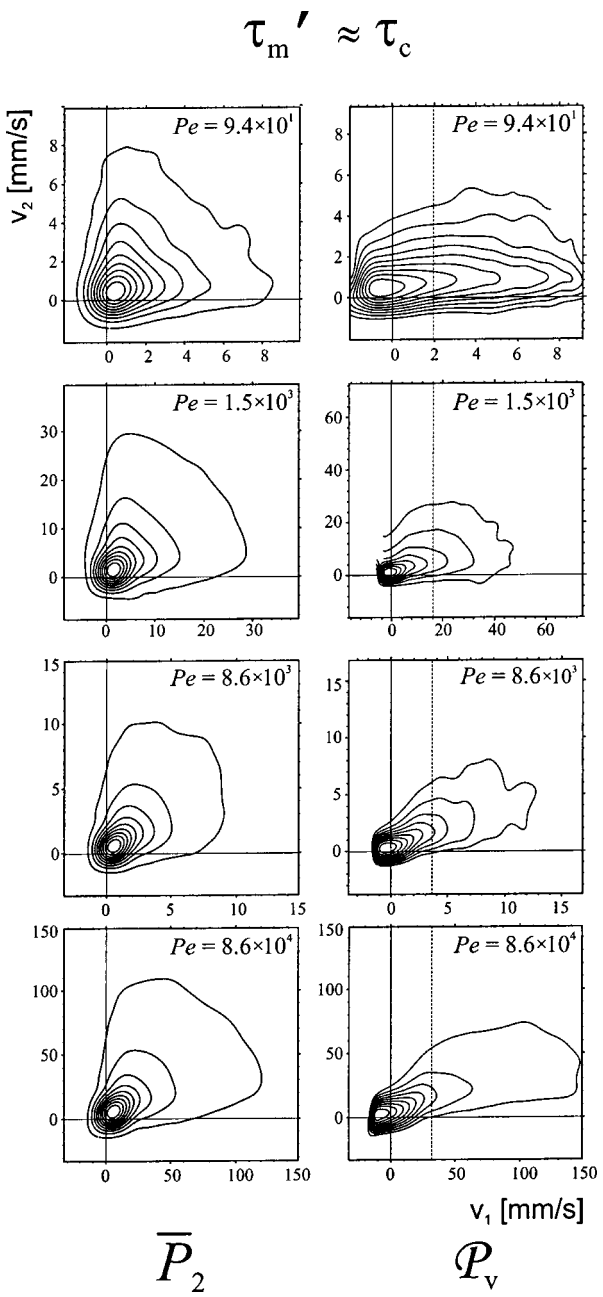

FIG. 12. Two-time joint probability density of velocities, $\bar{P}_2(Z_1,Z_2;\tau_m)$ (left-hand side), and conditional probability $\mathcal{P}_V(Z_1,\Delta|Z_2,\Delta;\tau_m)$ (right-hand side) for water and a water-glycerol mixture, flowing through packed beads of 100, 400, 500, and 500 μm diameter, respectively. All four experiments correspond to reduced effective mixing times $\tau_m'/\tau_c=(\tau_m+\Delta)/\tau_c$ between 1.0 and 1.1. Vertical lines on the right-hand side of the figures indicate flow displacements accumulated during $\tau_m'=\tau_c$, which are equal to the bead diameter. Contour lines are in steps of 10% where the peak amplitude is normalized to unity.

of $\mathcal{P}_v(Z_1,\Delta|Z_2,\Delta;\tau_m')$ becomes much more prominent, allowing a distinction between spins of different flow properties. For comparison, vertical lines in the right-hand part of Fig. 12 indicate the initial velocity v_1 for which $v_1\tau_m'=d$. These lines represent particles that have traveled a distance equal to the bead diameter over the mixing time, assuming they all kept their initial velocity. Because $\tau_m'=\tau_c$ in all four plots of Fig. 12, according to the definition of τ_c, the lines coincide with the average velocity of all particles, $\langle v\rangle$. The lines also separate those fluid elements for which the individual correlation time is smaller than the average τ_c (faster elements) from those larger than the average τ_c (slower elements). The different behavior of the two classes of fluid elements is most apparent at the highest Pe value of 8.6×10^4. While the faster moving elements have experienced velocity changes such that a correlation between the initial and final velocity is weak, corresponding to near-horizontal contour lines in the plot of the conditional probability, the slower elements tend to reside on the same streamline during the mixing time τ_m' and thus show contour lines with a positive slope, representing a positive correlation between v_1 and v_2.

The differing shapes of the conditional probabilities as one progresses through increasing Pe values on the right-hand side of Fig. 12 is especially interesting. They graphically illustrate that the approach to asymptotic conditions depends not just on the reduced mixing time τ_m'/τ_c but also on the Peclet number.

CONCLUSION

A specially designed NMR pulse sequence (VEXSY) has been applied for the systematic investigation of the temporal correlations of fluid motion during flow processes in structured media. The VEXSY technique is noninvasive and can be applied to opaque systems. Unlike other methods, it is able to encode displacements of spin-bearing molecules repeatedly and to time correlate their velocities in a statistical manner. Furthermore, this method can be used to calculate the experimental conditional probability function relating the displacements of molecules over separated time intervals. It is clear from the present study that this two-dimensional function can be used to graphically illustrate velocity correlations over an effective mixing time τ_m'. The degree of positive slope is a measure of correlation while horizontal contour lines correspond to uncorrelated displacements.

The present study allows us to draw some conclusions regarding dispersion in random bead packs. First, it is clear that both the Peclet number and the reduced mixing time τ_m'/τ_c are needed to define the conditional probability. Second, we observe a noticeably sigmoidal character to the conditional probability at preasymptotic mixing times. This suggests the existence of three ''pools'' of molecules, a slow moving uncorrelated subensemble whose displacement is dominated by Brownian motion, an intermediate ensemble whose velocities change little over τ_m', and a fast flowing ensemble which loses correlations due to mechanical dispersion. The very existence of separate ensembles argues against the description of fluid dispersion in terms of a simple single-correlation-time Ornstein-Uhlenbeck process. Third, we note that the approach to asymptotic dispersion depends strongly on the Peclet number, and not just on the reduced mixing time τ_m'/τ_c. As τ_m'/τ_c is increased, asymptotic conditions are most rapidly achieved at lowest Pe, where Brownian motion and Taylor dispersion are presumably most influential.

NMR is shown here to be a highly flexible technique that can give access to a wide range of hydrodynamic conditions. A feature of the present work concerns our coverage of three orders of magnitude of Peclet numbers up to 10^5, exceeding values reported in the existing literature. We suggest that the use of the two-dimensional VEXSY method can provide an effective qualitative tool for investigating the structural of velocity fluctuations in a graphic manner. The VEXSY technique can therefore provide a powerful tool for the investigation of flow transport problems in structured media. More complex applications might be found in the fields of biomedical research, chemical engineering, as well as oil and water recovery, where the ability of NMR to combine velocity information with chemical information provides a unique opportunity to study single-component and multicomponent flow in natural rocks.

ACKNOWLEDGMENTS

The authors are grateful to the New Zealand Foundation for Research, Science and Technology for funding support. S.S. is grateful to K. J. Packer and P. M. Adler for their support throughout the process of performing the numerical simulations for the porous medium. Part of this work was undertaken during a stimulating stay of S.S. at Victoria University, Wellington.

APPENDIX

The observation of flattened off-diagonal contours at high mixing times, as apparent in Fig. 6, appears to be anomalous. One of the basic assumptions of the analysis is that the displacements of all fluid elements are taken into account with their proper weighting. The experiment, however, is performed in such a way that all spins contribute to the signal, which remain within the volume of the receiver coil throughout the experiment. The coils used in these experiments possessed a length of 15 mm for the large bead packing and 10 mm for the small bead packing, respectively. Assuming a rectangular sensitivity profile along the flow axis, it becomes inevitable that a certain fraction of spins will leave the resonator during the total time of the pulse sequence, which is on the order of $2\Delta+\tau_m$ (neglecting the length of the gradient pulses themselves because of $\delta \ll \Delta$). Of all spins with a given average velocity $v=(v_1+v_2)/2$, a fraction $(2\Delta+\tau_m)v/L$ leaves the resonator of length L and does not contribute to the acquired signal. It is obvious that this affects the fastest fluid elements most, so that the distribution of velocities obtained by the VEXSY experiment becomes biased towards a larger weighting of slow molecules. This bias is negligible as long as $(2\Delta+\tau_m)v_{\max}/L \ll 1$, where $v_{\max}$ represents the highest particle velocity in the flow field, averaged between both encoding intervals. However, it contributes to the flattening of the outermost contour lines and their orientation along the secondary diagonal of the VEXSY plot, as the probability of leaving the resonator is equal for constant total displacements. It can thus be understood that the outermost contour lines, representing a small fraction of particles, give rise to a triangular pattern when their total displacement becomes a non-negligible fraction of the resonator length. As is seen in the simulated data in Fig. 9, for certain velocity distributions, such as the typical shape found for fluid flow through bead packs and $\Delta/\tau_c < 1$ (see Fig. 4), a tendency towards an approximately triangular shape of the VEXSY plot for long mixing times already appears even in the absence of outflow. The outflow effect enhances this flattening, which becomes obvious by comparing the experimentally obtained data (Fig. 8) with the simulated ones.

[1] R. A. Waggoner and E. Fukushima, Magn. Reson. Imaging **14**, 1085 (1996).
[2] K. J. Packer and J. J. Tessier, Mol. Phys. **87**, 267 (1998).
[3] P. Mansfield and B. Issa, J. Magn. Reson., Ser. A **122**, 137 (1996).
[4] S. H. Chen, F. F. Qin, K. H. Kim, and A. T. Watson, AIChE J. **39**, 925 (1993).
[5] J. J. Tessier and K. J. Packer, Phys. Fluids **10**, 75 (1998).
[6] U. Tallarek, D. van Dusschoten, H. Van As, E. Bayer, and G. Guiochon, J. Phys. Chem. B **102**, 3486 (1998).
[7] U. Tallarek, E. Bayer, and G. Guiochon, J. Am. Chem. Soc. **120**, 1494 (1998).
[8] J. Park and S. J. Gibbs, AIChE J. **45**, 655 (1999).
[9] L. F. Gladden, Top. Catal. **8**, 87 (1999).
[10] M. D. Mantle, A. J. Sederman, and L. F. Gladden, Chem. Eng. Sci. **56**, 523 (2001).
[11] J. Kärger and W. Heink, J. Magn. Reson. (1969-1992) **51**, 1 (1983).
[12] P. T. Callaghan, *Principles of Nuclear Magnetic Resonance Microscopy* (Clarendon, Oxford, 1991).
[13] J. Stepisnik, Prog. Nucl. Magn. Reson. Spectrosc. **17**, 187 (1985).
[14] A. J. Sederman, M. L. Johns, P. Alexander, and L. F. Gladden, Chem. Eng. Sci. **53**, 2117 (1998).
[15] E. Fukushima, Annu. Rev. Fluid Mech. **31**, 95 (1999).
[16] B. Blümich, *NMR Imaging of Materials* (Oxford University Press, Oxford, 2000).
[17] H.-P. Müller, J. Weis, and R. Kimmich, Phys. Rev. E **52**, 5195 (1995).
[18] A. Klemm, R. Kimmich, and M. Weber, Phys. Rev. E **63**, 041514 (2001).
[19] P. T. Callaghan, S. L. Codd, and J. D. Seymour, Concepts Magn. Reson. **11**, 181 (1999).
[20] A. Caprihan and J. Seymour, J. Magn. Reson. **144**, 96 (2000).
[21] P. T. Callaghan and J. Stepisnik, J. Magn. Reson., Ser. A **117**, 118 (1995).
[22] P. T. Callaghan and S. L. Codd, Phys. Fluids **13**, 421 (2001).
[23] P. T. Callaghan and B. Manz, J. Magn. Reson., Ser. A **106**, 260 (1994).
[24] S. Stapf, R. A. Damion, and K. J. Packer, J. Magn. Reson. **137**, 316 (1999).
[25] B. Blümich, P. T. Callaghan, R. A. Damion, S. Han, A. A. Khrapitchev, K. J. Packer, and S. Stapf, J. Magn. Reson. **152**, 162 (2001).
[26] A. A. Khrapitchev and P. T. Callaghan, J. Magn. Reson. **152**, 259 (2001).
[27] D. L. Koch and J. F. Brady, J. Fluid Mech. **180**, 387 (1987).
[28] D. L. Koch, Chem. Eng. Sci. **42**, 1377 (1987).
[29] J. F. Brady, *Hydrodynamics of Dispersed Media*, edited by J. P. Hulin, A. M. Cazabat, E. Guyon, and F. Carmona (Elsevier, New York, 1990).
[30] J. Bear, *Dynamics of Fluids in Porous Media* (American Elsevier, New York, 1972).
[31] S. Whitaker, Transp. Porous Media **1**, 3 (1986).
[32] O. A. Plumb and S. Whitaker, *Dynamics of Fluids in Hierarchical Porous Media*, edited by J. H. Cushman (Academic, San Diego, 1990).
[33] M. Quintard and S. Whitaker, Chem. Eng. Sci. **48**, 2537 (1993).
[34] J. Koplik, S. Redner, and D. Wilkinson, Phys. Rev. A **37**, 2619 (1988).
[35] J. Salles, J.-F. Thovert, R. Delannay, L. Prevors, J.-L. Auriault, and P. M. Adler, Phys. Fluids A **5**, 2348 (1993).
[36] D. Coelho, J.-F. Thovert, and P. M. Adler, Phys. Rev. E **55**, 1959 (1997).
[37] C. W. Gardiner, *Handbook of Stochastic Methods for Physics, Chemistry and the Natural Sciences*, 2nd ed. (Springer, New York, 1990).
[38] E. O. Stejskal and J. E. Tanner, J. Chem. Phys. **42**, 288 (1965).
[39] S. Han, S. Stapf, and B. Blümich, J. Magn. Reson. **146**, 169 (2000).
[40] S. Stapf, S. Han, C. Heine, and B. Blümich, Concepts Magn. Reson. **14**, 172 (2002).
[41] S. Stapf, J. Magn. Reson. **152**, 308 (2001).
[42] Y. Cheng and D. G. Cory, J. Am. Chem. Soc. **121**, 7935 (1999).
[43] P. T. Callaghan, S. L. Codd, and J. D. Seymour, Concepts Magn. Reson. **11**, 181 (1999).
[44] P. T. Callaghan and A. A. Khrapitchev, Magn. Reson. Imaging **19**, 301 (2001).
[45] S. Stapf, K. J. Packer, R. G. Graham, J.-F. Thovert, and P. M. Adler, Phys. Rev. E **58**, 6202 (1998).
[46] S. Stapf, K. J. Packer, S. Békri, and P. M. Adler, Phys. Fluids **12**, 566 (2000).
[47] D. Coelho, J.-F. Thovert, and P. M. Adler, Phys. Rev. E **55**, 1959 (1997).
[48] R. Lemaitre and P. M. Adler, Transp. Porous Media **5**, 325 (1990).
[49] J. J. Tessier, K. J. Packer, J.-F. Thovert, and P. M. Adler, AIChE J. **43**, 1653 (1997).
[50] Y. E. Kutzovsky, L. E. Scriven, H. T. Davis, and B. E. Hammer, Phys. Fluids **8**, 863 (1996).
[51] L. Lebon, J. Leblond, and J. P. Hulin, Phys. Fluids **9**, 481 (1997).
[52] L. Lebon, L. Oger, J. Leblond, J. P. Hulin, N. S. Martys, and L. M. Schwartz, Phys. Fluids **8**, 293 (1996).
[53] D. L. Koch and J. F. Brady, J. Fluid Mech. **154**, 399 (1985).
[54] P. N. Sen and M. D. Hürlimann, J. Chem. Phys. **101**, 5423 (1994).
[55] M. H. G. Amin, S. J. Gibbs, R. J. Chorley, K. S. Richards, T. A. Carpenter, and L. D. Hall, Proc. R. Soc. London, Ser. A **453**, 489 (1997).
[56] J. D. Seymour and P. T. Callaghan, AIChE J. **43**, 2096 (1997).
[57] R. Maier, D. M. Kroll, H. T. Davis, and R. Bernard, Phys. Fluids **10**, 60 (1998).
[58] R. S. Maier, D. M. Kroll, R. S. Bernard, S. E. Howington, J. F. Perters, and H. T. Davis, Phys. Fluids **12**, 2065 (2000).
[59] A. J. Sederman, M. L. Johns, P. Alexander, and L. F. Gladden, Magn. Reson. Imaging **16**, 497 (1998).